Title: Influence of floods, tides, and vegetation on sediment retention in Wax Lake Delta, LA, USA

Authors: E.A. Olliver[1], D.A. Edmonds[1], and J.B. Shaw[2]

[1]Department of Earth and Atmospheric Science, Indiana University, Bloomington, IN, USA

[2]Department of Geosciences, University of Arkansas, Fayetteville, AR, USA

*corresponding author, eolliver@indiana.edu

Key Points

1. Use numerical modeling to analyze sediment retention on a delta for various flood-wave magnitudes, tidal amplitudes, and vegetation extents

2. Vertical accretion increases with flood size, but sediment retention decreases, and tides increase retention during large floods

3. Vegetation reduces accretion and sediment retention on the delta due to the greater influence of buffering effect versus the trapping effect

Abstract

Sediment is the most valuable natural resource for deltaic environments, and to build new land sediment must be retained in the delta instead of being transported offshore. Despite this, we do not know what controls sediment retention within a delta. Here we use a calibrated numerical model of Wax Lake Delta, LA, USA to analyze sediment retention for different flood-wave magnitudes, tidal amplitudes, and vegetation extents. We only model transport of silt since it comprises most of the incoming sediment load. Our results show that as flood size increases, areally-averaged vertical accretion increases from 0.33 cm to 2 cm, but this comes at a cost because delta-scale sediment retention decreases from 72% to 34%. On a fully vegetated delta, we show that the buffering effect of vegetation reduces island-directed sediment flux by 14 to 22% because sediment takes the less resistive path in the channel. When sediment gets onto the islands, the trapping effect of vegetation increases retention by ~10%. But, this is not enough to offset the buffering effect, and vegetation decreases vertical accretion and sediment retention across the delta reduces by up to ~0.5 cm and 6%, respectively. We suggest that vegetation will increase sedimentation only when trapping compensates for buffering. Finally, greater tidal amplitude at higher discharges enhances vertical accretion by ~0.5 cm per flood as compared to a minimum tidal amplitude condition. These results inform how coastal deltaic systems grow and

suggest how to operate sediment diversions more efficiently in deltas with reduced sediment supply.

1. Introduction

Sediment retention is a key unknown in the delta building process. Obviously, sediment must be deposited nearshore for delta building to occur, but we know little about what controls how much of the incoming sediment is retained for delta building and how much is transported out of the delta. The simplest way to quantify retention is as the fraction of sediment deposited relative to the total input over a given time interval (Paola et al., 2011). It is critical that we understand the controls on sediment retention because sediment delivery to most deltas is being reduced. For example, on the Mississippi River, the installation of dams has reduced sediment transport downstream and construction of containment levees has limited the overbank flooding and deposition necessary for wetland sustainment (Stanley & Warne, 1993; Syvitski et al., 2005, 2007; Yang et al., 2005; Blum & Roberts, 2009; Meade & Moody, 2010). As a result, over the past 80 years this sediment starvations has contributed to the conversion of ~5000 km^2 of land into open water (Couvillion et al., 2011). Given these losses, it has become widely accepted that coastal restoration in Louisiana must focus on maximizing land building and reducing additional land loss. Despite the reduction in sediment loads to the coast, some river systems still transport enough sediment to build new deltaic wetlands, such as the Atchafalaya and Wax Lake deltas within the greater Mississippi River Delta (MRD) (Roberts et al., 2003; Rosen & Xu, 2013; Carle et al., 2015). Thus, a central component of coastal restoration plans in Louisiana is strategic placement and operation of freshwater and sediment diversions, which emulate the natural processes of crevassing and deltaic land building (CPRA, 2017). Crucially, diverting water and sediment into desired areas does not guarantee land building. Land building will only

occur when sediment is retained within the delta, and successful diversions should aim to maximize sediment retention.

Sediment retention depends on the processes that supply and remove sediment in a deltaic system. We divide these processes into continuous or episodic. The continuous processes include riverine discharge, the presence of vegetation, tides, and waves. Of these continuous processes, field measurements over days to months indicate that riverine discharge is the primary control of sediment delivery to the system, which is important for eventual sediment retention (Fabre, 2012; Day et al., 2016a; Allison et al., 2017; Keogh et al., 2019). Previous work has shown vegetation enhances sediment deposition and retention in both salt marshes and deltaic freshwater marshes by decreasing water flow velocities, enhancing bed roughness, and directly capturing sediment in the vegetation canopy (Leonard & Luther, 1995; Christiansen et al., 2000; Neumeier & Ciavola, 2004; Gedan et al., 2011; Fagherazzi et al., 2012; Nardin & Edmonds, 2014; Nardin et al., 2016; Ma et al., 2018; Larsen, 2019). However, in some instances, vegetation has also been shown to act as a buffer, directing the flow of sediment laden water away from vegetated areas (Nardin & Edmonds, 2014; Nardin et al., 2016; Temmerman et al., 2005, 2007).

While we have some sense of how water discharge and vegetation influence retention, relatively little is known about waves and tides. In the paired observational and numerical modeling study by Allison et al. (2017), they determined from fluorescent tracers that retention of the riverine sediments in the West Bay receiving basin was more evenly distributed in space than predicted by the modeling results. Allison et al. (2017) suggested this more even distribution could be due to influence of tides, waves, or wind-driven currents. While Allison et al. (2017) did not measure or model tidal processes, there is conjecture that tides maybe

104 important for sediment retention (Hiatt et al., 2019). Analyses of process connectivity in Wax
105 Lake Delta indicates tidal influence is greatest at the delta shoreline and decreases updelta
106 (Sendrowski & Passalacqua, 2017). However, because Wax Lake Delta is relatively small, the
107 tidal influence could be important because it extends further updelta than in a larger, more
108 heterogeneous system like the MRD. The resuspension of sediment by wind-driven waves has
109 been identified as a key process transporting sediment in shallow bays and estuaries in the MRD
110 (Lane et al., 2007; Wang et al., 2018), resulting in sediment transport in and out of deltaic
111 environments. Additionally, edge erosion by waves can result in degradation of existing deltaic
112 marshes (Day et al., 2011; Mariotti, 2016; Ortiz et al., 2017).

113 The aforementioned processes are more or less continuously operating, and there are
114 other episodic processes, such as hurricanes and seasonal cold fronts, that influence sediment
115 retention in the MRD. Southerly and easterly winds of an approaching cold front can result in a
116 net influx of water into coastal bays and wetlands with resulting inundation of 30-50 cm (Denes
117 & Caffrey, 1988; Childers & Day, 1990). Winds shift to westerly and northerly as cold fronts
118 pass, resulting in rapid drainage of the flooded wetlands. The inundation and draining caused by
119 these cold fronts in autumn and winter results in the transport of sediment, nutrients, and organic
120 matter among coastal bays, adjacent wetlands, and the Gulf of Mexico (Madden et al., 1988;
121 Childers & Day, 1990; Stern et al., 1991; Perez et al., 2000). Despite this, the role of cold fronts
122 in building deltaic land is relatively understudied. However, on WLD Bevington et al. (2017)
123 showed that during a winter cold front season, sediment was eroded from the deltaic islands.
124 Large storm surges associated with hurricanes occurring between June and November can result
125 in significant deposition and erosion of wetlands (Turner et al., 2006; Day et al., 2007). For
126 example, Hurricanes Katrina and Rita resulted in the conversion of ~100 km^2 of wetlands in the

Breton Sound Basin to shallow marsh with erosion of more than 1 m in some areas, while other areas saw 5-10 cm of deposition (Day et al., 2007). Numerical simulations of Hurricanes Katrina and Rita and their impact on the WLD indicate wave action produced significant erosion (Xing et al., 2017). Despite the constructive and destructive force of hurricanes, Smith et al. (2015) reported long-term sediment deposition due to hurricanes to be significantly less than what is supplied by fluvial sources.

These continuous and episodic processes also vary in time and space, which has an important influence on retention. This means that the retention fraction depends on the temporal and spatial scales. For example, in a study of the West Bay diversion in the MRD, Allison et al. (2017) reported a riverine sand retention of nearly 100% over two weeks. However, this retention rapidly decreased to 40% after multiple months. This decrease in the retention fraction is likely the result of sediment escaping the system at longer time scales (Xu et al., 2019). Similarly, sediment retention should increase when measured over larger spatial scales, but there is no widely agreed upon definition of the seaward boundary for a receiving basin (Xu et al., 2019). On the temporal side, the seasonal and intra-annual variability of water and sediment discharge strongly influences the magnitude of sediment retention for various years or periods of a given year (Day et al., 2016a,b; Peyronnin et al., 2017). On Davis Pond in the MRD, the sediment retention changed from 44% during winter/spring to 81% during summer/fall (Keogh et al., 2019). The lower winter/spring retention fraction likely results from the higher water velocities observed during that period, keeping more sediment in suspension and decreasing water residence over the basin (Keogh et al., 2019). Keogh et al. (2019) also suggested the seasonally variability in vegetation presence likely increased retention from the winter/spring to summer/fall.

Despite these studies, we still lack an understanding of how these forcing mechanisms interact to retain sediment within a delta. This knowledge gap is of theoretical and practical importance, because understanding how these forces interact would inform how coastal deltaic systems grow and help operate planned sediment diversions more efficiently. Field-based approaches have illustrated just how variable sediment retention can be in time and space (Fabre, 2012; Day et al., 2016a; Allison et al., 2017; Esposito et al., 2017; Keogh et al., 2019), and an important next step is to study the problem with a numerical model where the data is higher resolution in time and space, and where cause and effect can be more easily isolated. Here we present a calibrated numerical model of Wax Lake Delta built in Delft3D and use it to analyze how sediment retention varies for different flood-wave magnitude, tidal amplitude, and extent of vegetation coverage on the existing deltaic islands. We choose to assess the influence of these three forcing mechanisms because they are continuous in nature, and are the primary drivers of flooding of the deltaic islands. We choose to ignore waves in this study because they are small in the Gulf of Mexico and minimally affect sediment transport around Wax Lake Delta and onto the deltaic islands (Wright & Coleman, 1973,1974). We are interested in how changes in the magnitude of our forcing mechanisms affect sediment retention magnitude and distribution. We calculate the sediment retention for the whole delta and assess the spatial distribution of this retained sediment across subsections (basin, delta front, channels, and islands).

2. Study area

The Wax Lake Delta (WLD) is an actively prograding bayhead delta within the greater MRD system. Located at the mouth of the Wax Lake Outlet (WLO), WLD resulted from anthropogenic diversion of the Atchafalaya River in 1941. First becoming emergent in 1973, WLD experienced rapid growth in the following years due to record flooding in 1973 and 1975

(Van Heerden & Roberts, 1988). Upon aggrading to an elevation where overlying water was shallow enough, ruderal plant species have colonized the deltaic islands (Carle et al., 2015). WLD has continued to grow vertically and laterally (Roberts et al., 2003; Kim et al., 2009) Rosen & Xu, 2013; Carle et al., 2015; Olliver & Edmonds, 2017) in a coastal wetland system with some of the highest land-loss rates in the world (Gagliano et al., 1981; Day et al., 2000; Couvillion et al., 2011). While perhaps an unintended product of the Atchafalaya River diversion, WLD serves as an example of what the diversions proposed in Louisiana's Coastal Protection and Restoration Authority (CPRA) Master Plan hope to accomplish (CPRA, 2017). Its role as a natural field observatory and use as a template in numerical modeling studies can provide insight into how wetlands in these systems develop and what controls sediment retention in them.

3. Methods

3.1 Modeling domain

To assess the impact of floods, tides, and vegetation on sediment retention within a deltaic system, we constructed a hydrodynamic model of the WLD in Delft3D. Our model of WLD uses a 20 m resolution seamless DEM as the initial bathymetry (Figure 1a). We constructed this DEM using LiDAR data of the subaerial islands collected as part of the USGS Atchafalaya 2 LiDAR campaign (NOAA, 2015), single beam bathymetry of the delta front collected in February 2015 and multi-beam bathymetry in the distributary channels collected in 2007, 2009, and 2013 (Shaw et al., 2016; their supplementary material). The 20 m resolution of our seamless DEM captures the primary channel and island features of the delta, and the smaller channels within the deltaic islands (Figure 1a, inset). Our modeling domain has an upstream boundary where we specify the incoming water discharge and suspended sediment and

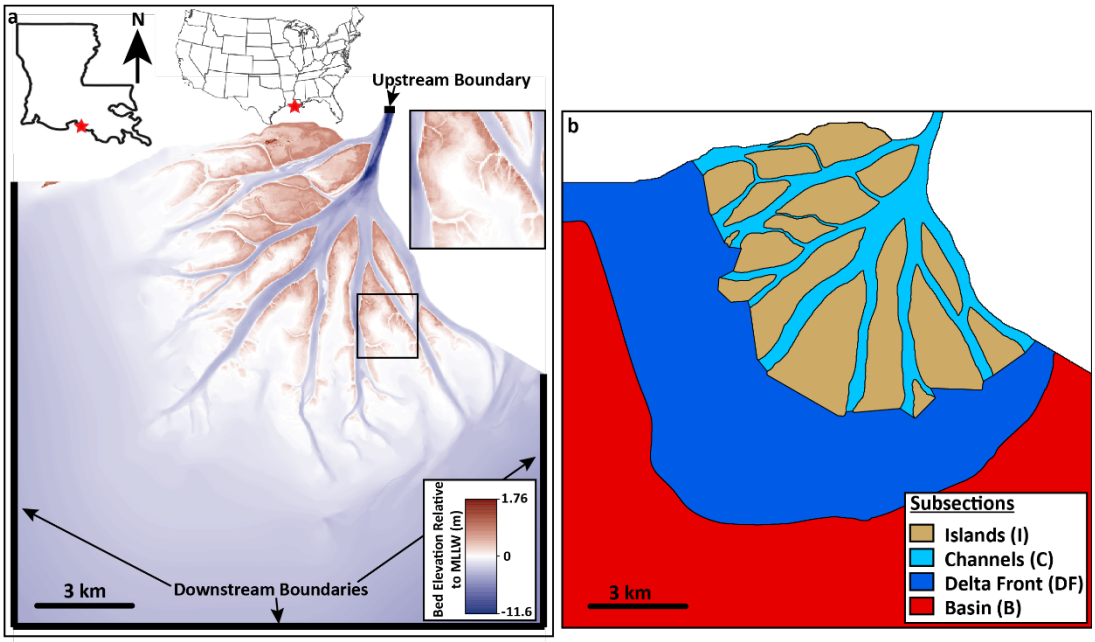

Figure 1 – (a) Modeling domain and digital elevation model (DEM) of the Wax Lake Delta, LA, USA. The red star marks the location of our study area in Louisiana. DEM resolution is 20 m x 20 m and the upstream and downstream model boundaries are marked by bold black lines. The inset image displays how the DEM resolves the primary features of the delta and also the smaller channels in the island interiors. (b) Subsections of the modeling domain used for sediment retention and areally-averaged vertical accretion calculations.

downstream boundaries where we specify the water level fluctuations due to tides (Figure 1a). We populate the island tops with vegetation of consistent height (1 m) and stem density (0.25 m^{-1}), which is calculated assuming ~25 stems per square meter and a stem diameter of ~1 cm. The stem diameter is typical of *Typha latifolia* (Kadlec & Wallace, 2008), a common species in WLD (Johnson et al., 1985). While our spatial density is lower than the ~40 stems per square meter typical of *Typha latifolia* (Grace, 1989; Miller & Fujii, 2010), this density is an intermediate value within the range of stem density considered by Nardin et al., (2016). The interaction between flow and vegetation is governed by the Baptist (2005) formulation. In this study, we use two vegetated extent maps, which represent the areal vegetation coverage at minimum and maximum biomass periods of the year, as well as a no vegetation extent map (Figure 2a,b). The minimum and maximum vegetated extent maps are based on work presented by Olliver & Edmonds (2017).

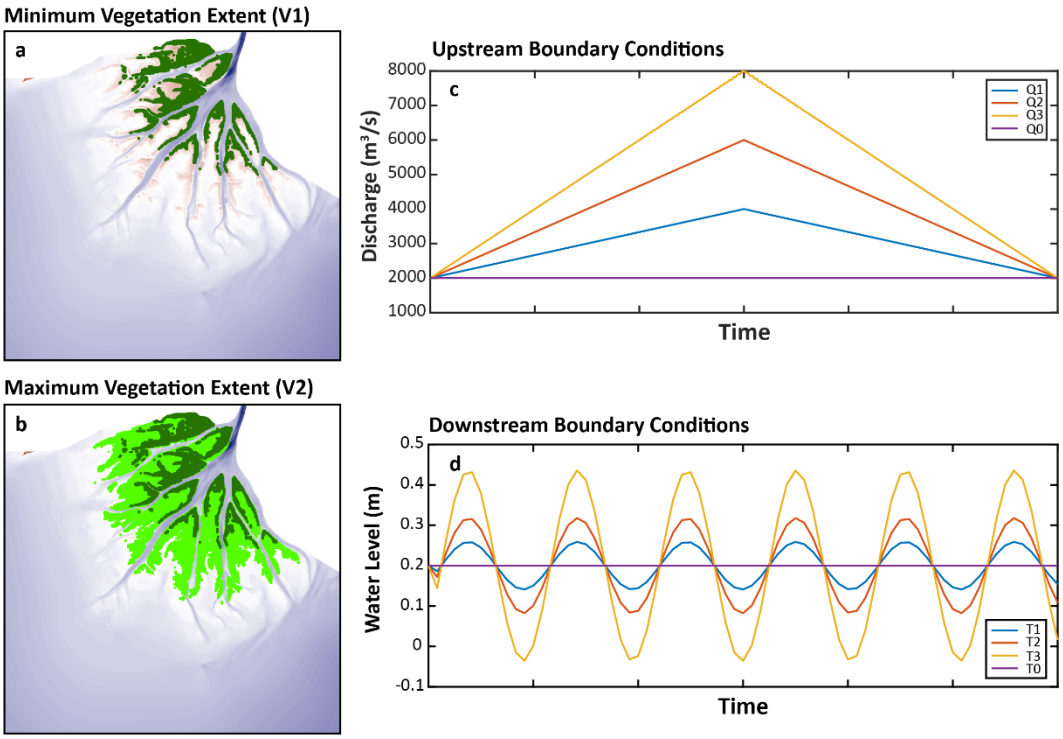

Figure 2 – (a-b) The extent of vegetation coverage on the deltaic islands with constant vegetation height (1m) and density (0.25 m^{-1}) between and throughout for our minimum (V1) and maximum (V2) vegetation extent runs. (c) The flood waves and (d) tidal amplitudes applied at the upstream and downstream boundary, respectively.

3.2 Model calibration and validation

We calibrated our model using field-collected water depths from several platforms located in the interior of an island of WLD (Figure 3a). For calibration we used water depths from April and September, representing the minimum and maximum biomass, respectively (Figure 2a,b), from three platforms (Figure 3b-g). The calibration model runs were forced with

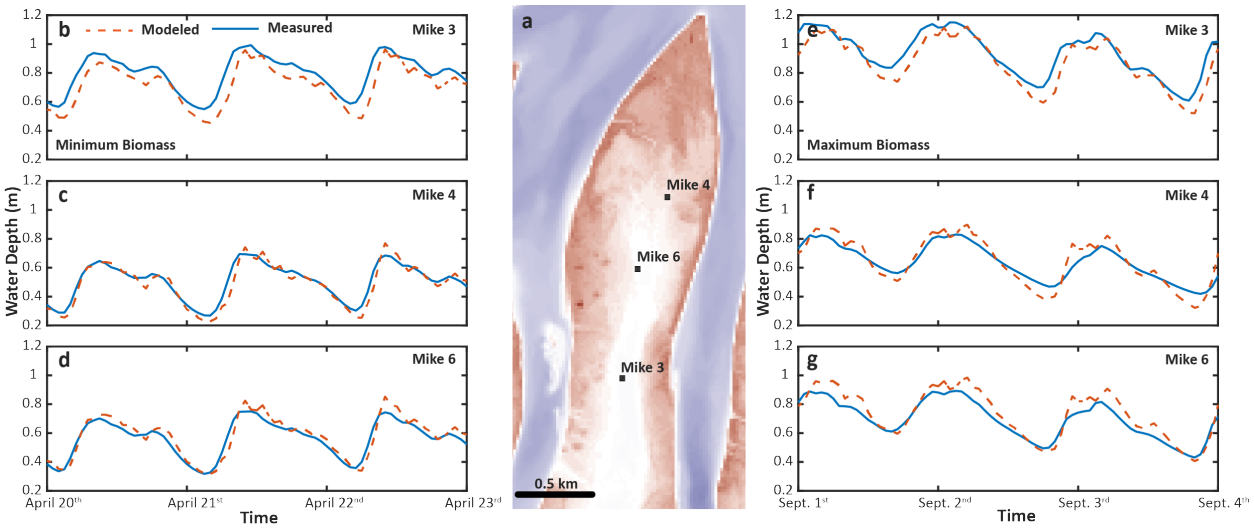

Figure 3 – (a) Location of the observation platforms within the interior of Mike Island in WLD. Model calibration results for minimum biomass (b-d) and maximum biomass (e-g) shows good agreement between observed water-depth data observed (solid line) and modeled (dashed line).

the water discharge (USGS Calumet gauge on the WLO; Gauge 07381590) and the tidal water levels (NOAA Amerada Pass in the Atchafalaya Delta; Gauge 8764227) over the same time period as the water-depth data was collected. We calibrated the water level in the model to an average root mean square error of 0.06 m between the measured and modeled data (Figure 3b-g). We accomplished this by using different Manning's roughness of n = 0.01 for the channels, unvegetated interdistributary bays, and delta front, and an n = 0.2 for areas populated by subaerial vegetation (dark green area, Figure 2a), and an n = 0.08 for the vegetated intertidal zone (light green area, Figure 2b). We also had to raise the downstream tidal water levels by 0.2 m. This suggests that the gauge in Amerada Pass may not faithfully represent the tidal level in neighboring WLD nearly 15 km away. This is not surprising given that the gauge is located within the channel network of the Atchafalaya Delta, and tidal waves are transformed as they funnel through distributary networks and interact with fluvial discharge (Hoitink & Day, 2016).

To validate the model, we compared model output to measured water depths in 72 locations that were not used in the calibration. From August 20th to August 23rd, 2014, we

collected water depths at discrete points (Olliver & Edmonds, 2017) (Figure 4a). Using the calibrated model, we ran a simulation over the same time period our water-depth data were collected using upstream water discharge from the USGS Calumet gauge and downstream tidal conditions from Amerada Pass with a 0.2 m increase. We then compared the water depth predicted by the model at the exact time we collected the water-depth data in the field. Our calibrated model predicted water depths with a RMSE = 0.08 m as compared to the observed water-depth data across the deltaic islands (Figure 4).

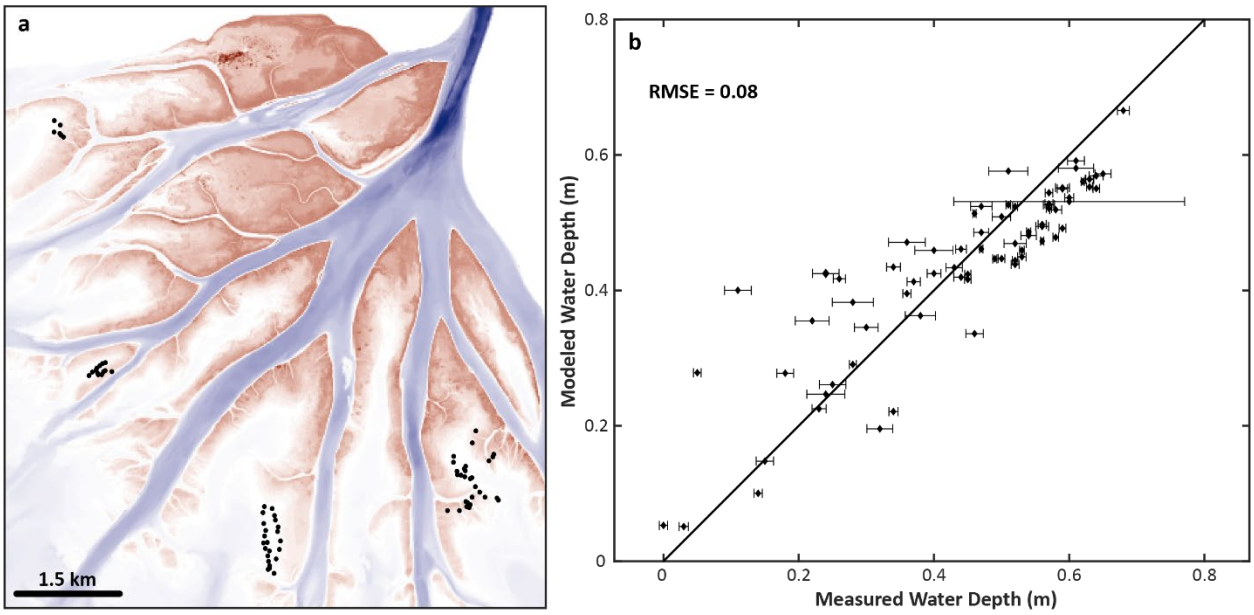

Figure 4 – (a) Locations of water depth measurements used for model validation. (b) Measured water depths at locations presented in (a) versus the model-predicted water depths. Solid black line represents a 1:1 fit. Our model accurately predicts water depth to with 8 cm of the observed water depth. The horizontal error bars represent variance of bed elevation within the 20 m cell in which each data point is located as determined using the original 5 m resolution seamless DEM.

3.3 Experimental design and choice of boundary conditions

Our modeling is designed to understand how incoming flood-wave magnitude, tidal amplitude, and the extent of island vegetation coverage affects sediment retention. One approach would be to drive the model with measured hydrographs from the Calumet gauge, and tidal fluctuations from Amerada Pass, but that introduces additional variables we are difficult to

control for, such as hydrograph shape or tidal irregularities. Instead, we designed the boundary conditions to be generically representative of these processes. This way we could smoothly vary the magnitude of these boundary forcings over parameter space, which allows us to more clearly understand cause and effect.

In our model runs the flood-wave magnitude varies over four conditions: a no flood wave condition but constant discharge of 2000 m^3s^{-1} (*Q0*), to three different triangular flood waves with a base discharge of 2000 m^3s^{-1} and peak discharges of 4000 m^3s^{-1} (*Q1*), 6000 m^3s^{-1} (*Q2*), and 8000 m^3s^{-1} (*Q3*) (Figure 2c). The *Q0* condition is the average base flow during the spring flood period. Our range of peak discharges are an evenly distributed sampling of low, medium, and high magnitude flood discharges based on the range of discharges observed at the USGS Calumet gauge from 1987 to 2018. We simplify the tidal signal to just the semi-diurnal component and vary over it four conditions: no tide but constant base level of 0.2 m relative to MLLW (*T0*) to three semi-diurnal tides with amplitudes of 0.059 m (*T1*), 0.118 m (*T2*), and 0.236 m (*T3*) (Figure 2d). The *T0* condition is the water-level adjustment to our downstream boundary made during model calibration. The range of tidal amplitudes for conditions *T1* to *T3* are determined from the range of semi-diurnal components measured at the Amerada Pass gauge, which we center on our baseline of 0.2 m relative to MLLW.

The sixteen combinations of discharge and tidal conditions were run for three different vegetation conditions for a total of 48 model runs. Vegetated extent of the islands varies from a null condition of unvegetated (*V0*) to minimum (*V1*) and maximum vegetated extent (*V2*) (Figure 2a,b). For *V0*, the alluvial bed roughness is n = 0.01 everywhere. For *V1*, the dark green areas (Figure 2a) have n = 0.2, and for *V2*, the light green areas have n = 0.08 (Figure 2b). All other areas in *V1* and *V2* have n = 0.01. Vegetation, where present, always has a constant height (1 m)

and stem density (0.25 m^{-1}). This choice is clearly a simplification because, although vegetation communities are more complex, we simplified the height and density so that we could focus on how vegetation extent affects sediment retention.

We introduce silt (59 μm) and freshwater at the upstream boundary over the duration of the model runs. The basin is assumed to contain freshwater throughout the run. The concentration of silt suspended silt is set by an empirically-derived relationship between discharge and suspended sediment concentration from data collected in the WLO by the USGS (Figure A1). We only consider the silt fraction and ignore sand because silt makes up ~91% of the sediment entering WLD (Shaw et al., 2013). In addition, since the system is relatively mature the islands are nourished primarily by silt that is carried higher in the water column, as opposed to the sand that remains in the channels. We set a grain settling velocity of 3 mm s^{-1}. Using Ferguson and Church (2004) this corresponds to an unflocculated grain size of 59 μm. Based on this settling velocity, we set the critical bed shear stress for sedimentation to 0.01 N m^{-2}. This corresponds to a shear velocity of approximately 3 mm/s, in this way when the bed shear stress is below this value, grain settling exceeds the shear velocity and sedimentation can occur. For simplicity, we eliminate the possibility of erosion or re-suspension of the silt after deposition by setting the critical bed shear stress for erosion at 100 Nm^{-2}, though tests for select model runs indicate this does not change the results. Delf3D calculates suspended load transport by solving the diffusion-advection equation. As we use cohesive sediment in our model, the Partheniades-Krone formulations for erosion and deposition were used (Partheniades, 1965). In Delft3D we set out minimum depth for sediment calculation to 0.1 m. We ran our models for three days model time, with a morphological scale factor of 20 applied so the runs represent 60 days of bed evolution. This 60-day period represents the median duration of a flood pulse down the WLO

based on visual inspection of the Calumet gauge discharge records for the winter/spring flood seasons from 1987 to 2018.

We assessed how the silt moves through the deltaic system by dividing the modeling domain into four subsections based on hydrological and ecogeomorphic attributes: the distributary channel network (C), deltaic islands (I), delta front (DF), and the basin (B) (Figure 1b). The boundary between the channel network and island areas is the wet/dry boundary at the bankfull discharge of ~2000 m^3s^{-1}. We consider the boundary between each island and the delta front to be the minimally convex hull spanning the two most distal points of vegetated area at maximum biomass. This boundary also roughly coincides with the 0 m relative to MLLW elevation contour. The channel-delta front boundary was defined as a series of minimally convex hulls spanning from the two most distal points of vegetated areas of neighboring islands. Finally, the basin-delta front boundary is set at the -2 m relative to MLLW elevation contour based on work presented by Geleynse et al. (2015).

3.4 Analyses of model runs

For our analyses, we calculate four different quantities that describe retention at different scales. First, we calculate the porosity-adjusted volume of sediment deposited in each subsection ($D_{subsection}$, m^3) relative to the total incoming silt measured at the upstream boundary (D_o, m^3), a term we refer to as delta-scale retention ($F_{subsection}$) (Equation 1):

$$F_{subsection} = \frac{D_{subsection}}{D_0} * 100 \qquad \text{(Equation 1)}$$

Delta-scale, in this sense, refers to the total incoming sediment flux at the upstream boundary and subscript *subsection* refers to one of the four subsections in Figure 1b. Second, for

only the islands, we calculate the total incoming silt onto the islands ($D_{o,I}$, m^3) relative to D_o, a term we refer to as potential delta-scale retention on the islands ($F_{I,P}$) (Equation 2):

$$F_{I,P} = \frac{D_{o,I}}{D_o} * 100 \quad \text{(Equation 2)}$$

$D_{o,I}$ is calculated by finding the component of the sediment flux vector perpendicular to the boundary of the island for each model grid cell and summing them all. Third, we calculate the total porosity-adjusted volume of sediment deposited on the islands (D_I, m^3) relative to $D_{o,I}$, which is the island-scale retention (f_I) (Equation 3):

$$f_I = \frac{D_I}{D_{o,I}} * 100 \quad \text{(Equation 3)}$$

The areally-averaged vertical accretion on the islands resulting from this silt retention was also calculated ($\overline{\Delta d}_I$, cm) (Equation 4):

$$\overline{\Delta d}_I = \frac{D_I}{A_I} * 100 \quad \text{(Equation 4)}$$

where A_I (m^2) is the total area of the islands.

4. Results

The results presented here focus on model runs using the *V0* and *V2* vegetated extents (Figure 2a,b). We conducted runs using the *V1* extent, but as we discuss later, these results are nearly identical to *V0* (Table 1). Here we show results illustrating how retention varies at the delta-scale and as a hydrodynamic drivers of river discharge, and tidal amplitude. The effects of vegetation are discussed in the sections of river discharge and tidal amplitude.

4.1 Delta-scale retention

The percentage of silt retained within all the delta subsections ($F_D = F_I + F_C + F_{DF}$) across our test parameters decreases from 72 to 34% (unvegetated, *V0*) and from 66 to 34% (max-vegetated, *V2*) with increasing flood-wave magnitude (*Q0* to *Q3*) (Figure 5). In fact, increasing Q decreases the proportion of sediment in the topset ($F_I + F_C$) while the proportion retained in F_{DF} increases (Figure 5, Table 1). This occurs because at higher Q the higher flow velocities

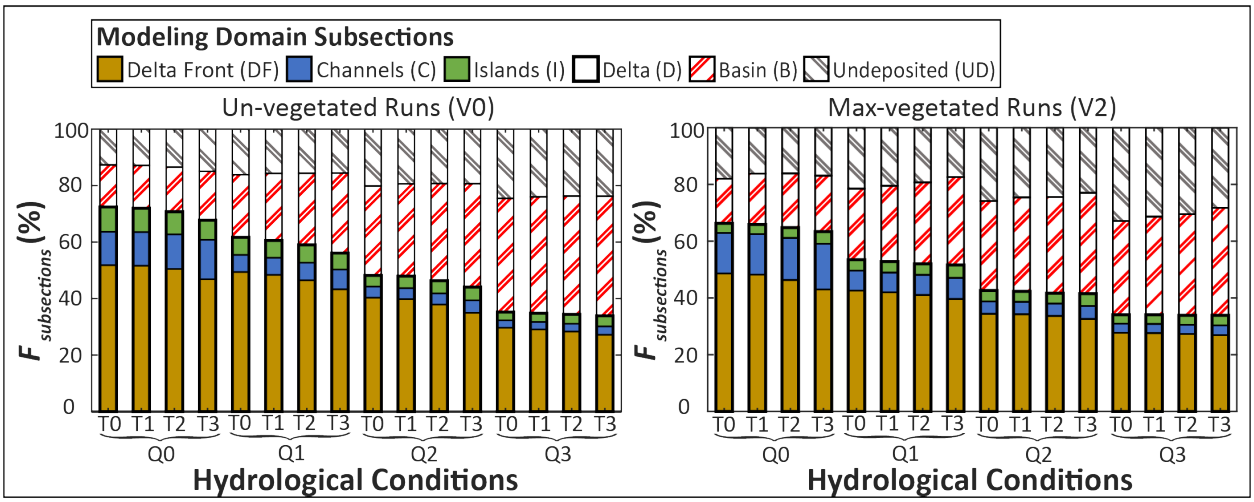

Figure 5 – Delta-scale silt retention (F) for each modeling domain subsection for each of our (a) unvegetated (V0) and (b) max-vegetated (V2) runs. Along the x-axis, each grouping of four is a flood wave condition (Q0-3), with each bar in a grouping a tidal condition (T0-3). On the y-axis, the bars are divided into the proportional amounts of D_o for each given run retained in each domain subsection. The undeposited subsection represents the proportion of D_o that has exited the domain or remains in suspension at run conclusion.

cause sediment to bypass the delta topset. As a result, silt retention in the basin (F_B) increases with Q from 15 to 42% (*V0*) and 16 to 38% (*V2*). The proportion of D_o that exits the domain at the downstream boundary or remains in suspension when the run ends (F_{UD}) also increases from 13 to 24% (*V0*) and 18 to 28% (*V2*) with increasing Q (Figure 5, Table 1).

An increase in tidal amplitude (*T0* to *T3*) reduces delta-scale retention, F_D, by 3 to 5% at *Q0*, but by only ~1.5% at *Q3* (Figure 5, Table 1). Most of this reduction is accommodated by decreasing F_{DF} with increasing Q. But interestingly, F_C and F_I have a more variable response and show increases or decreases with increasing Q at different vegetative conditions (Table 1).

364 The presence of vegetation reduces F_D from ~6% at *Q0* to ~0.5% at *Q3* (Figure 5, Table
365 1). Specifically, from *V0* to *V2* retention in the delta front (DF) and islands (I) decreases by 1 to
366 4% and 0.5 to 5%, respectively, while retention in the channels (C) increases by 0.5 to 3%.
367 Conversely, vegetation increases retention in the basin (B) from 1 to 5%, as well as the
368 proportion of D_o that remains undeposited (from 2 to 8%). However, regardless of flood-wave
369 magnitude, tidal amplitude, or vegetation, the majority of sediment retained within the delta is
370 deposited in the delta front (52 to 27%), followed by the channels (14 to 3%) and islands (8 to
371 3%) (Figure 5; Table 1).

372 Surprisingly, there is almost no difference in retention for the *V0* and *V1* condition across
373 our runs (Table 1). This suggests to us that, as least for the range of parameters considered in this
374 study, the minimal vegetation condition behaves like a completely unvegetated delta.

375 **4.2 The role of flood-wave magnitude**

376 The amount of sediment that flows onto the deltaic islands is an interesting quantity since
377 deltaic islands make up the subaerial landscape, and to keep pace with relative sea-level rise they
378 must be nourished by sediment. $F_{I,P}$ is the proportion of sediment that flows onto the islands and
379 we call it the potential retention because it is the maximum amount of sediment that could be
380 deposited. The difference between the potential retention for the *V0* and the *V2* conditions
381 ($F_{I,P}\big|_{V0} - F_{I,P}\big|_{V2}$) is a quantity we term as the vegetation buffering effect (Figure 6; length of
382 dashed grey arrow denotes magnitude of buffering effect). For a given vegetation condition, the
383 difference between incoming sediment and deposited sediment ($F_{I,P}$ - F_I) is the percentage of silt
384 (relative to D_o) is not deposited, something we term silt loss (Figure 6; length of dashed black
385 arrow denotes magnitude of silt loss). The $F_{I,P}$ and F_I results cluster according to flood-wave

magnitude and vegetated extent, and each cluster contains four points that correspond to different tidal amplitudes (Figure 6; $F_{I,P}$ and F_I clusters outlined by dashed and solid lines, respectively).

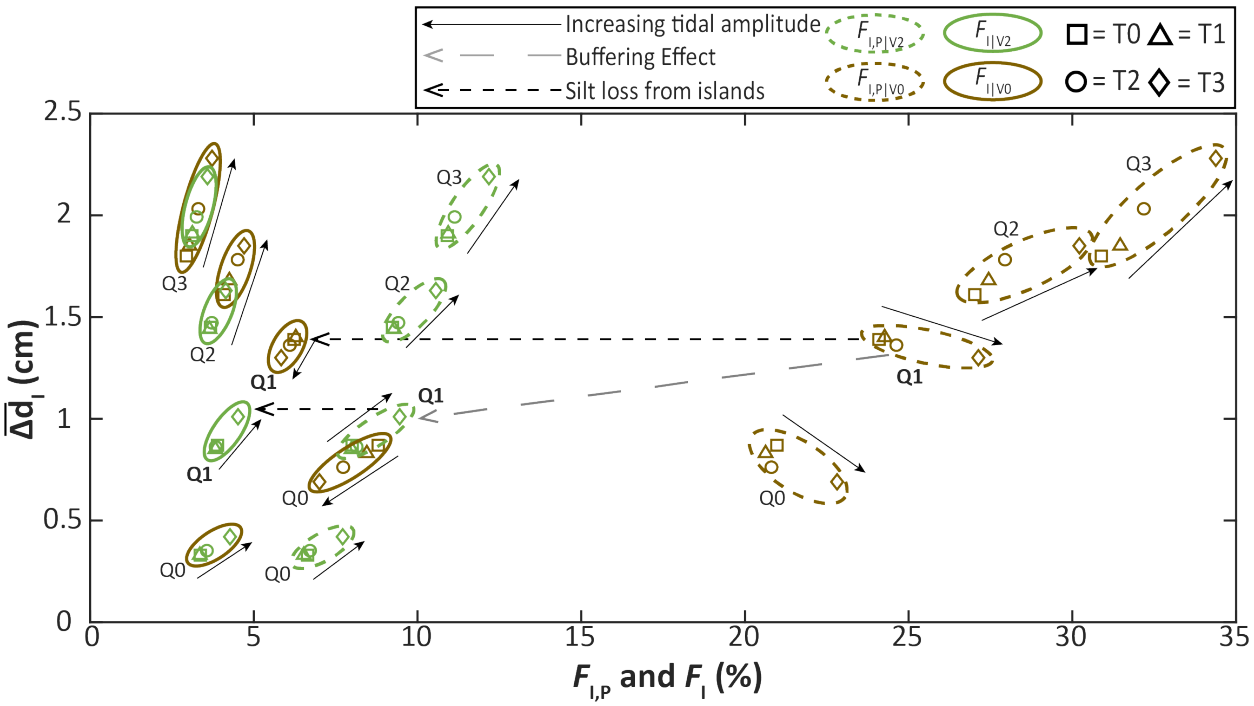

Figure 6 – The relationship between sediment retention and accretion at the delta-scale. The data clusters are labeled by flood wave conditions (*Q0-3*) and outlined by dashed and solid lines for the $F_{I,P}$ and F_I data, respectively. The brown or green color of the cluster outlines denotes the *V0* and *V2* condition, respectively. The dashed grey arrow denotes the buffering effect, whereas the dashed black arrows denote the loss of silt from the islands. Similar lines could be drawn along all runs but are omitted for clarity. The solid black arrows alongside each $F_{I,P}$ and F_I grouping highlights the trend of increasing tidal amplitude.

The magnitude of the buffering effect ($F_{I,P}|_{V0} - F_{I,P}|_{V2}$) changes as a function of discharge. As Q increases, so do $F_{I,P}$ and $\overline{\Delta d}_I$ for both the *V0* and *V2* runs because larger floods transport more sediment onto the islands. However, the *V2* runs have lower $\overline{\Delta d}_I$, and much lower $F_{I,P}$, compared to *V0*. Thus, at *Q0* the buffering effect reduces $F_{I,P}$ by roughly 14%, whereas at *Q3* the buffering effect reduces $F_{I,P}$ by about 20% (Figure 6, Table 2). If we view the buffering effect proportionally then $\frac{Q_{s,I}|_{V2}}{Q_{s,I}|_{V0}} \approx 67\%$ for nearly all runs. The consistency of this proportion is likely because we do not vary vegetation parameters, such as height and density, among our runs.

As Q increases, the percentage of sediment deposited in the islands, F_I, decreases, while $\overline{\Delta d}_I$ increases (Figure 6). This is especially true for the *V0* condition. This negative trend is opposite of the positive trend for $F_{I,P}$ and this arises because silt loss increases with higher Q (Figure 6; dashed black arrow). Even though $F_{I,P}$ increases at higher Q, there is less retention on the islands because increased water depths and velocities across the islands advect more sediment off them. The data for *V2* show similar behavior, but the silt loss ($F_{I,P}\big|_{V2} - F_I|_{V2}$) at a given Q is not as great as *V0* because vegetation increases sediment retention by decreasing sediment advection off the islands.

The tendency of vegetation to increase sediment retention is something we term the trapping effect. Though we do not directly measure the trapping effect, it is the complementary percentage with silt loss (dashed black arrow, Figure 6, Table 2). For both *V0* and *V2*, the quantity $F_{I,P} - F_I$ increases with Q. But importantly, both the magnitude of silt loss and the increase in silt loss with increasing Q is much greater for the *V0* condition than for the *V2* condition (Figure 6; Table 2). The consistently smaller decrease from $F_{I,P}$ to F_I for the *V2* condition shows how vegetation contributes to silt retention.

To consider the trapping effect more directly, we shift our perspective and consider island-scale retention (f_I), which is sediment deposition relative to the sediment flux onto the islands ($D_{o,I}$) rather than relative to the total sediment entering the deltaic system at the upstream boundary (D_o). From this perspective, vegetation increases retention (~28 to 55%) compared to the unvegetated condition (~9 to 42%) for a given flood-wave magnitude and tidal amplitude (Figure 7). f_I decreases with greater flood-wave magnitude for *V0* and *V2*, which underscores that while vegetation enhances silt retention on the islands, this trapping effect becomes less effective at higher Q.

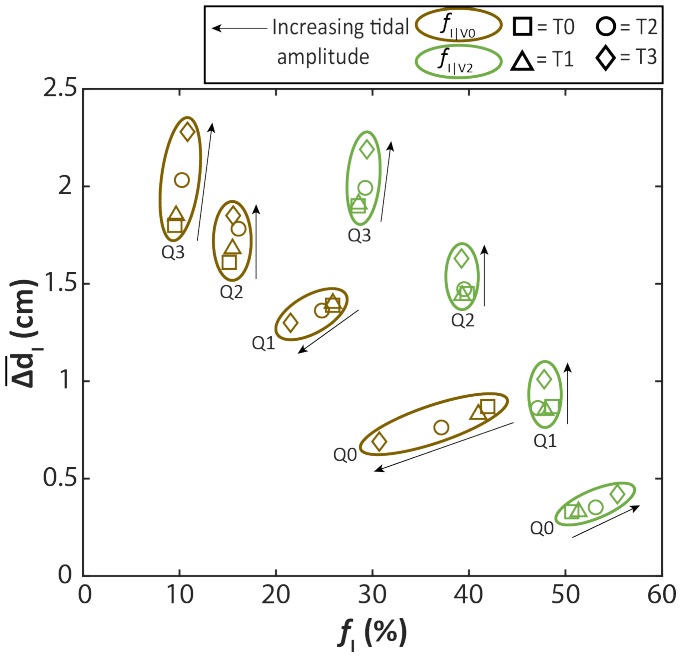

Figure 7 – The relationship between sediment retention and accretion at the island-scale. The data groupings are labeled by flood-wave conditions (*Q0-3*) and outlined by solid brown and green lines denoting the *V0* and *V2* runs, respectively. The solid black arrow alongside each f_I grouping highlights the trend of increasing tidal amplitude.

4.3 The role of tidal amplitude

As already discussed, each *Q* and vegetation condition cluster contains four points that correspond to different tidal amplitudes (Figures 6 and 7). Tidal amplitude has a smaller influence on silt retention over the entire delta (Figure 5) and within the deltaic islands (Figures 6 and 7), compared to flood-wave magnitude or the presence of vegetation. But, the effect of tidal amplitude is not monotonic; in some cases tides increase retention and in other cases they decrease it.

Regardless of vegetation or flood-wave magnitude, tides increase $F_{I,P}$ by roughly 1 to 3% for *V0* and *V2* conditions (Figure 6). This occurs because greater tidal amplitude increases island inundation and transports more silt onto the islands. However, as tides recede, they also transport suspended silt out of the islands and this effect can offset the increase in $F_{I,P}$. Notice that for most of our runs, greater tidal amplitude results in greater F_I or f_I (Figures 6 and 7). However, for

the *V0* condition at *Q0* and *Q1* the opposite is true, and lower tidal amplitude results in greater silt retention (Figures 6 and 7). This reversal never occurs for the *V2* condition.

This reversal does not occur for *V2* because the trapping effect of vegetation limits sediment export from the islands as the tide recedes. To see this, we plot the instantaneous and cumulative net silt flux from each model timestep (Figure 8). We define net silt flux as the total silt flux into the islands minus the amount that fluxes out of the islands. At *Q0* runs with tides in

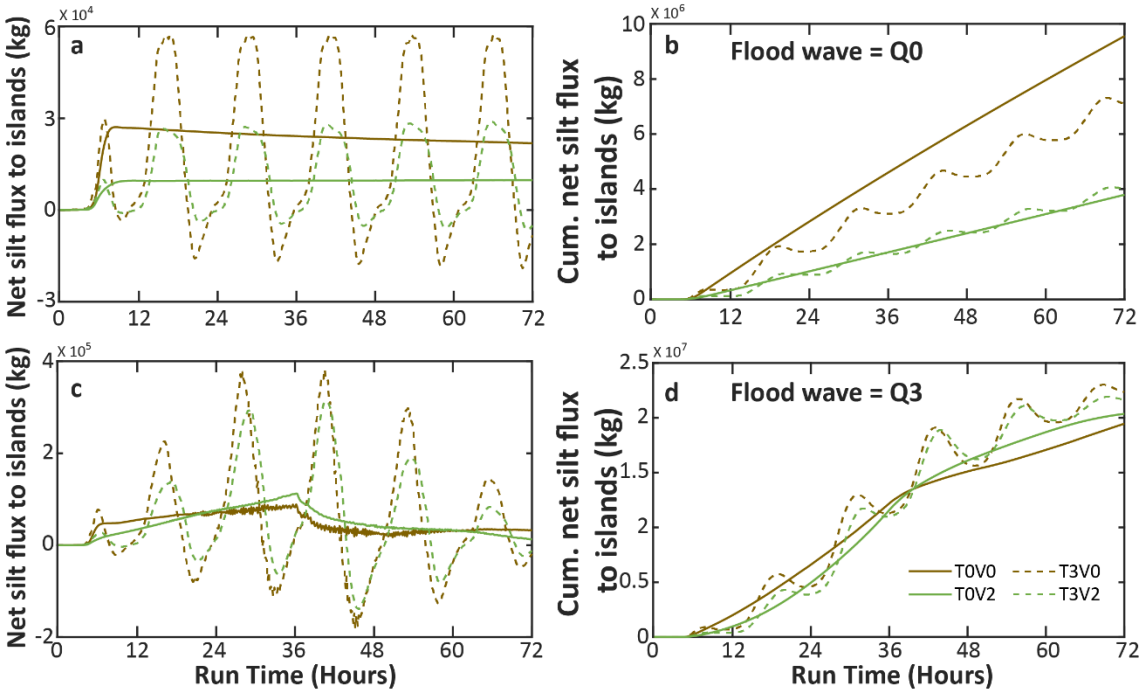

Figure 8 – (a,c) Instantaneous net silt flux to all islands over the course of the runs for the null (*T0*, solid) and max tidal amplitude (*T3*, dashed) and for the null (*Q0*) and max flood wave (*Q3*). (b,d) Cumulative net silt flux over the course of the aforementioned runs. Both the unvegetated (*V0*, brown) and vegetated (*V2*, green) conditions for these flood wave and tidal amplitude end member runs are presented.

the absence of vegetation (*T3V0*) result in higher instantaneous net flux compared to the no tide condition (*T0V0*), but also result in periods of negative instantaneous net flux when more silt leaves the islands than enters (Figure 8a). When no tide is present (*T0V0*, *T0V2*), the instantaneous net silt flux remains at a lower but consistently positive value. The cumulative net silt flux shows that the increased flux during high tide does not offset the sediment exported

457 during low tide, and the result is that tides lower the cumulative flux at *Q0* and *V0* conditions
458 (Figure 8b; dashed brown line is below solid brown line). But for the *V2* conditions, the trapping
459 effect of vegetation reduces silt loss from the islands and the benefit of tides outweighs the
460 detriment, creating a small increase in cumulative net flux (Figure 8a,b; dashed green line is
461 slightly above the solid green).

462 At *Q3* however, the enhanced silt delivery to the islands offsets the loss caused by tides,
463 even in the absence of vegetation. The *V0* and *V2* condition show similar values of net
464 instantaneous flux at high and low tide (Figure 8d). Initially, the cumulative fluxes for all
465 conditions are also similar, but by 60 hours of model runtime the cumulative flux for runs with
466 tides becomes larger than without tides, indicating the net benefit of tides at higher *Q* (Figure 8d;
467 dashed brown and green lines are higher than corresponding solid lines at the end of the run).

468 **5. Discussion**

469 **5.1 How the competing effects of buffering and trapping govern the vegetation**
470 **sedimentation feedback**

471 One of the prevailing notions in ecogeomorphology is that, all else being equal, the
472 presence of above-ground vegetation on the marsh surface can enhance sediment deposition by
473 reducing turbulence and flow velocities in the water column, which promotes the settling of
474 sediment out of suspension (Leonard & Luther, 1995; Christiansen et al., 2000; Morris et al.,
475 2002; Neumeier & Ciavola, 2004; Kirwan & Murray, 2007; Fagherazzi et al., 2012). This
476 enhanced sedimentation does not always occur because sparse vegetation can increase turbulence
477 and limit deposition (Larsen, 2019). Vegetation also reduces bed shear stress thereby limiting
478 remobilization of sediment following initial deposition (Christiansen et al., 2000; Howes et al.,

2010). The tendency of vegetation to enhance sedimentation is often formalized as a positive feedback (Larsen, 2019), especially in models of salt marshes (Kirwan & Murray, 2007; Fagherazzi et al., 2012 and references therein) and fluvial floodplains (Kleinhans et al., 2018 and references therein), where the presence of vegetation, up to a point, causes faster rates of vertical surface accretion. This positive vegetation-sedimentation feedback in our study is manifested as the sediment trapping effect. Another well-documented effect of vegetation is the occurrence of a stress-divergence feedback. As water interacts with an isolated patch of vegetation, the difference of roughness between the vegetation and the smoother bed surrounding it causes stress to diverge and concentrates flow along the patch margins where there is less resistance (Weerman et al., 2010; Temmerman et al., 2005, 2007; Nardin & Edmonds, 2014; Nardin et al., 2016; Larsen, 2019; Yamasaki et al., 2019 and references there in). This can lead to erosion at the patch margin, further concentration of flow, and eventual channelization. While we did not simulate planform development and channelization in our model, this stress-divergence feedback is the mechanism in our runs that creates the buffering effect, which reduces sediment transport onto the islands due to the presence of vegetation (Weerman et al., 2010).

The trapping and buffering effects together determine whether vegetation causes an increase or decrease in sedimentation in a morphodynamic system. An interesting result of our modeling experiments is that in all scenarios tested here, vegetation is ultimately a negative feedback and results in less sedimentation (*V2* clusters always have equal or less $\overline{\Delta d}_I$ than *V0* clusters, Figures 6 and 7). This stands in contrast to previous studies where vegetation causes an increase in sedimentation compared to unvegetated conditions (Kirwan & Murray, 2007; Fagherazzi et al., 2012; Larsen, 2019). This arises in our results because the buffering effect is always larger than the trapping effect for our chosen vegetation height and density conditions.

The buffering and trapping effects can be tracked on Figure 6 by following the trajectory from $F_{I,P}\big|_{V0} \rightarrow F_{I,P}\big|_{V2} \rightarrow F_I|_{V2}$ for any given discharge condition. For example, at *Q1* $F_{I,P}\big|_{V2}$ is less than $F_{I,P}\big|_{V0}$ because of the buffering effect (Figure 6, dashed grey arrow). The amount retained on the isalnds, $F_I|_{V2}$, is lower than the incoming flux $F_{I,P}\big|_{V2}$ (Figure 6, dashed black arrows) because some silt is lost from the islands. For *Q0*, *Q1*, *Q2* the combined effects of buffering ($F_{I,P}\big|_{V0} \rightarrow F_{I,P}\big|_{V2}$ dashed gray line) and silt loss from the islands ($F_{I,P}\big|_{V2} \rightarrow F_I|_{V2}$ dashed black arrow) are always larger than the silt loss for unvegetated conditions ($F_{I,P}\big|_{V0} \rightarrow F_I|_{V0}$ dashed black arrow Figure 6). Because of this, the *V2* conditions have smaller F_I and $\overline{\Delta d}_I$ than *V0* conditions.

Consistent with general expectations for vegetated surfaces, at *Q1* the silt loss from the islands ($F_{I,P} \rightarrow F_I$) is greater for *V0* than *V2* because vegetation enhances sediment trapping. Interestingly, at *Q3* for both *V0* and *V2*, F_I and $\overline{\Delta d}_I$ are nearly identical. This suggests that at high discharge the trapping effect balances out the buffering effect. A reasonable conjecture would then be that at discharges higher than *Q3* vegetation might result in higher retention and more deposition. While this is sensible, the peak discharge for the *Q3* condition we model here (8000 $m^3 s^{-1}$) is nearly the maximum observed discharge at Wax Lake Outlet and does not recur often. Because of this, it seems unlikely that under reasonable hydrologic conditions vegetation will create higher sedimentation on WLD. However, we only used one set of vegetation characteristics in our runs and the interaction of the buffering and trapping effects may vary in relation to these characteristics (Nardin & Edmonds, 2014; Nardin et al., 2016). In addition, there are vegetation effects we do not simulate, such as direct capture (Strumpf, 1983; Yang et al., 2008; Larsen, 2019), which we assume is small compared to direct deposition.

Our model results imply the vegetation only enhances deposition over unvegetated conditions if the trapping effect overcomes the buffering effect. This balancing act between trapping and buffering is not usually considered or parameterized in models. This could be, in part, because many studies on vegetation and sedimentation focus on salt marsh environments (e.g., Fagherazzi et al., 2012 and references therein) where the buffering effect is minimized because sediment and water flow into a closed tidal basin. In closed tidal basins, water and sediment enter and exit through the same cross-section, and the presence of vegetation predominately affects the location along the tidal channel network that sediment enters the marsh, but not the total sediment flux onto the marsh surface (Temmerman et al., 2005, 2007). In deltaic marshes, on the other hand, the basin is not closed, and water and sediment can flow onto the marshes, or bypass them completely by flowing through the channel network and into the ocean.

Because deltas are not closed basins, an important next step is to map out the conditions where the trapping and buffering effects lead to enhanced or decreased sedimentation. In the runs we only used one set of vegetation characteristics, but previous work on a generic delta suggests that there may be optimal vegetation height and density where the trapping effect is greater than the buffering effect (Nardin & Edmonds, 2014; Nardin et al., 2016). Future work could try to map out buffering and trapping effects relative to one another and define when vegetation-sedimentation feedback in deltaic marshes is positive or negative. An important point to make, however, is that our experiments did not allow for erosion of the substrate or resuspension of sediment following initial deposition. This effectively maximizes the trapping effect, and if this limitation is relaxed then vegetation may produce an even more drastic decrease in sedimentation.

5.2 Operational considerations and trade-offs for sediment diversions

Efforts towards mitigation and reversal of wetland loss in coastal deltaic wetlands, like the MRD, often consider vertical accretion as a measure of success. Because vertical accretion is so important, inorganic sediment is one of the most valuable resources along disappearing coastlines. But, river management structures, like dams and levees, have reduced sediment supply to the coast making it important to achieve vertical accretion of the marsh platform with efficient sediment retention. As one might guess, in river-dominated deltas like the one studied here, big floods lead to significant sediment deposition in the delta and on the islands (Snedden et al., 2007; Kolker et al., 2012; Esposito et al., 2013; Rosenheim et al., 2013; Carle et al., 2015; Shen et al., 2015; Bevington et al., 2017). But, that comes at a tradeoff because as vertical accretion goes up, sediment retention goes down (Figures 6 and 7). Fieldwork by Keogh et al. (2019) showed similar results. Thus, while larger flood waves may enhance vertical accretion of existing wetlands (a desired outcome of sediment diversion construction), it comes at the cost of lower sediment retention in the delta.

Based on the fieldwork in the Davis Pond diversion, Keogh et al. (2019) proposed a conceptual model that suggests an optimal discharge range for sediment deposition, beyond which deposition will decrease. Our deposition results for the deltaic islands do not follow this conceptual model because deposition increases monotonically up to the highest magnitude flood wave WLD is likely to experience. The inconsistency between our results and the Keogh et al. (2019) conceptual model may be due to the differences in the scales of sediment retention discussed. Our results focus on deposition within the deltaic islands, while Keogh et al. (2019) considers deposition within the entire David Pond basin. Additionally, Keogh et al. (2019) developed the conceptual model based on data extrapolated from limited data (average

570 discharges for winter/spring and summer/fall for one year), which lie on the lower end of the
571 discharge range for the diversion. Thus, our results indicate for the WLD system higher rather
572 than intermediate discharges should be considered for diversion operations if the goal is to
573 maintain or aggrade existing wetlands.

574 Timing of operations is another important factor to consider when seeking to maximize
575 land-building potential of a sediment diversion. Peyronnin et al. (2017) suggested operational
576 strategies for the Mid-Barataria Sediment Diversion by identifying periods of the annual
577 hydrograph during which diversion operations would maximize land building while seeking to
578 limit detrimental impact to the existing ecosystem. Focusing diversion operations in the winter
579 and/or early spring to take advantage of the higher concentration of sand, silt, and clay typically
580 carried by the first peak of the water year (Peyronnin et al., 2017; Allison et al., 2012).
581 Operations later in the year should seek to operate the diversion on the rising limb of flood peaks
582 in order in order to capture as much sediment in the diversion as possible, per unit of freshwater
583 entering the diversion (Peyronnin et al., 2017). Additionally, Peyronnin et al. (2017) suggested
584 winter operation while vegetation is senesced could reduce vegetation stress and loss from
585 prolonged flooding. Our study further supports that operations be focused in the winter/early
586 spring period of the year, because during this period of the year larger magnitude discharges
587 occur and vegetation is senesced; both conditions create greater vertical accretion of existing
588 wetlands (Figures 6 and 7). However, it should be kept in mind, as stated earlier, maximizing this
589 vertical accretion will come at the cost of sediment retention due to greater throughput to the
590 basin. While more work is required on the subject, we note the suggestion by Peyronnin et al.
591 (2017) that cold fronts during the winter/spring could help maximize sediment resuspension and

592 transfer back onto wetland surface from the basin, which could help improve sediment retention
593 and further improve vertical accretion.

594 Finally, while perhaps the smallest influence considered in our study, our results show
595 tides have an important impact on sediment retention and deposition, even in the face of high
596 discharges (Figures 6 and 7). Consider that at *Q3* for the *V0* condition, the *T3* amplitude results
597 in a ~0.5 cm increase in $\overline{\Delta d}_I$ compared to *T1*. Thus at higher Q, tides enhance deposition with
598 minimal change to retention (Figures 6 and 7). In this way, if diversion operations are timed with
599 higher spring tides it could create more vertical accretion. Furthermore, larger tidal amplitudes
600 also may help mitigate sediment loss from the deltaic system by reducing higher flood velocities
601 that move sediment into the basin (Wright, 1977). F_{DF} decreases with greater tidal amplitude,
602 suggesting this reducing effect fails to retain more sediment on the distal edge of the delta (Table
603 1). However, F_B increases, while F_{UD} decreases with greater tidal amplitude, indicating greater
604 tidal amplitudes may be helping to retain more sediment in the basin adjacent to the delta and
605 possibly contribute to reduced transport of sediment offshore (Table 1). Finer spatial analyses of
606 where within the basin this retained sediment is deposited would help clarify this. It should also
607 be noted our delineation of the delta front/basin boundary was only one of various possible
608 definitions. A different boundary definition may place the boundary further seaward, resulting in
609 different F_{DF} and F_B trends, and thus points to the need for standardization and wide application
610 of the definition for the delta front/basin boundary in future studies.

611 **6. Conclusion**

612 In this study we used a calibrated numerical model of the Wax Lake Delta (WLD) to
613 consider how river discharge, tidal amplitude, and vegetation extent influence sediment
614 retention. The most important factor for sediment retention is river discharge because that is the

615 primary supplier of sediment. As discharge increases, vertical accretion of existing wetlands
616 increases, but sediment retention, relative to the total incoming flux, across the whole delta
617 decreases from 72 to 34% because more sediment bypasses the delta to the basin. This highlights
618 an important tradeoff for sediment-starved deltas: enhanced deposition comes at the expense of
619 lower retention.

620 We find that in all scenarios tested here vegetation is ultimately a negative feedback and
621 results in less vertical accretion of the islands and lower sediment retention than if vegetation is
622 not present or senesced. This occurs because of the interaction of the buffering and trapping
623 effects of vegetation. Buffering reduces sediment flux onto islands, whereas trapping enhances
624 deposition, and in our run the buffering effect is always greater than trapping. But, we only
625 modeled one vegetation condition and more study is needed to consider how variations in
626 vegetation height and/or density alter this outcome.

627 Larger tidal amplitudes increase vertical accretion at higher discharges and they may help
628 to reduce sediment bypass to the basin. Thus, our findings indicate timing of diversion operations
629 during higher amplitude tides, in the winter/spring months when discharges are typically higher
630 in the MRD system and vegetation is senesced may be best for maximizing vertical accretion of
631 existing wetlands.

632
633
634

Table 1 – Delta-scale silt retention ($F_{subsection}$) for *V0*, *V1*, and *V2* conditions. *V0* and *V2* data are shown in Figure 5. D = delta (DF + C +I), DF = delta front, C = delta channels, I = delta islands, B = basin, and UD = undeposited. See Figure 1b for the locations of domains, DF, C, I, and B.

	$F_{DF\|V0}$	$F_{DF\|V1}$	$F_{DF\|V2}$	$F_{C\|V0}$	$F_{C\|V1}$	$F_{C\|V2}$	$F_{I\|V0}$	$F_{I\|V1}$	$F_{I\|V2}$	$F_{D\|V0}$	$F_{D\|V1}$	$F_{D\|V2}$	$F_{B\|V0}$	$F_{B\|V1}$	$F_{B\|V2}$	$F_{UD\|V0}$	$F_{UD\|V1}$	$F_{UD\|V2}$
Q0T0	51.82	49.30	48.67	11.82	14.56	14.26	8.80	8.44	3.36	72.44	72.30	66.29	14.90	15.01	15.66	12.66	12.69	18.05
Q0T1	51.63	49.09	48.19	11.91	14.68	14.36	8.45	8.09	3.35	71.99	71.85	65.91	15.13	15.34	17.95	12.87	12.81	16.14
Q0T2	50.47	48.01	46.34	12.27	15.11	14.81	7.74	7.44	3.58	70.48	70.55	64.73	16.03	15.99	19.15	13.49	13.46	16.12
Q0T3	46.84	44.42	42.98	14.01	16.95	16.07	7.01	6.65	4.27	67.85	68.01	63.32	17.19	17.04	19.78	14.96	14.94	16.90
Q1T0	49.40	48.92	42.56	6.07	6.83	7.05	6.23	6.19	3.89	61.70	61.94	53.50	22.14	21.47	25.03	16.16	16.59	21.47
Q1T1	48.40	47.90	42.00	6.05	6.76	6.98	6.28	6.24	3.83	60.73	60.90	52.81	23.58	23.03	26.69	15.69	16.07	20.51
Q1T2	46.48	46.01	41.07	6.24	6.89	7.09	6.11	6.03	3.85	58.84	58.93	52.01	25.55	25.23	28.69	15.61	15.84	19.30
Q1T3	43.30	42.96	39.64	6.97	7.46	7.44	5.84	5.74	4.52	56.10	56.16	51.60	28.37	28.13	30.96	15.53	15.71	17.43
Q2T0	40.34	40.28	34.44	3.94	4.03	4.34	4.09	4.07	3.68	48.38	48.37	42.46	31.48	31.61	31.66	20.14	20.02	25.88
Q2T1	39.81	39.75	34.31	3.91	3.97	4.34	4.25	4.21	3.65	47.97	47.93	42.29	32.62	32.62	33.14	19.41	19.46	24.56
Q2T2	37.88	37.83	33.68	3.98	4.07	4.39	4.52	4.49	3.73	46.38	46.39	41.80	34.35	34.14	33.77	19.27	19.47	24.43
Q2T3	34.96	35.03	32.62	4.39	4.41	4.59	4.70	4.64	4.14	44.05	44.08	41.35	36.61	36.36	35.68	19.34	19.56	22.97
Q3T0	29.65	29.67	27.75	2.66	2.65	3.23	2.94	2.84	3.11	35.24	35.16	34.09	40.24	40.34	33.00	24.52	24.50	32.91
Q3T1	29.06	29.11	27.63	2.68	2.64	3.24	3.04	2.94	3.12	34.78	34.69	34.00	41.27	41.43	34.66	23.95	23.87	31.34
Q3T2	28.38	28.40	27.30	2.71	2.68	3.29	3.32	3.22	3.27	34.41	34.30	33.85	41.87	41.87	35.67	23.73	23.83	30.48
Q3T3	27.21	27.30	26.92	2.96	2.87	3.40	3.72	3.65	3.58	33.89	33.81	33.90	42.34	42.20	37.84	23.77	23.99	28.25

645 Table 2 – Average vertical accretion, and delta-scale (*F*) and island-scale (*f*) sediment retention for the *V0* and *V2* conditions. These data are plotted in Figures 6
646 and 7.

	$F_{I,P}\|_{V0}$	$F_{I,P}\|_{V2}$	Buffering effect $F_{I,P}\|_{V0} - F_{I,P}\|_{V2}$	$F_I\|_{V0}$	$F_I\|_{V2}$	Trapping Effect $F_{I,P}\|_{V0} - F_I\|_{V0}$	Trapping Effect $F_{I,P}\|_{V2} - F_I\|_{V2}$	$f_I\|_{V0}$	$f_I\|_{V2}$	$\overline{\Delta d}_I\|_{V0}$	$\overline{\Delta d}_I\|_{V2}$
Q0T0	20.98	6.64	14.33	8.80	3.36	12.18	3.28	41.95	50.65	0.87	0.33
Q0T1	20.63	6.52	14.11	8.45	3.35	12.18	3.17	40.97	51.35	0.83	0.33
Q0T2	20.82	6.73	14.09	7.74	3.58	13.08	3.15	37.19	53.18	0.76	0.35
Q0T3	22.81	7.72	15.10	7.01	4.27	15.80	3.45	30.70	55.38	0.69	0.42
Q1T0	24.09	8.00	16.09	6.23	3.89	17.86	4.11	25.87	48.60	1.39	0.87
Q1T1	24.27	7.99	16.28	6.28	3.83	17.99	4.16	25.89	47.90	1.40	0.85
Q1T2	24.64	8.15	16.48	6.11	3.85	18.53	4.30	24.81	47.18	1.36	0.86
Q1T3	27.13	9.45	17.67	5.84	4.52	21.29	4.93	21.51	47.79	1.30	1.01
Q2T0	27.02	9.24	17.79	4.09	3.68	22.93	5.56	15.15	39.81	1.61	1.45
Q2T1	27.44	9.28	18.16	4.25	3.65	23.19	5.63	15.50	39.28	1.68	1.44
Q2T2	27.95	9.43	18.53	4.52	3.73	23.43	5.70	16.17	39.55	1.78	1.47
Q2T3	30.21	10.56	19.65	4.70	4.14	25.51	6.42	15.57	39.22	1.85	1.63
Q3T0	30.88	10.91	19.98	2.94	3.11	27.94	7.80	9.52	28.51	1.80	1.90
Q3T1	31.46	10.94	20.52	3.04	3.12	28.42	7.82	9.65	28.56	1.85	1.91
Q3T2	32.20	11.15	21.05	3.32	3.27	28.88	7.88	10.30	29.30	2.03	1.99
Q3T3	34.38	12.18	22.20	3.72	3.58	30.66	8.60	10.83	29.42	2.28	2.19

647

Supplemental Figure

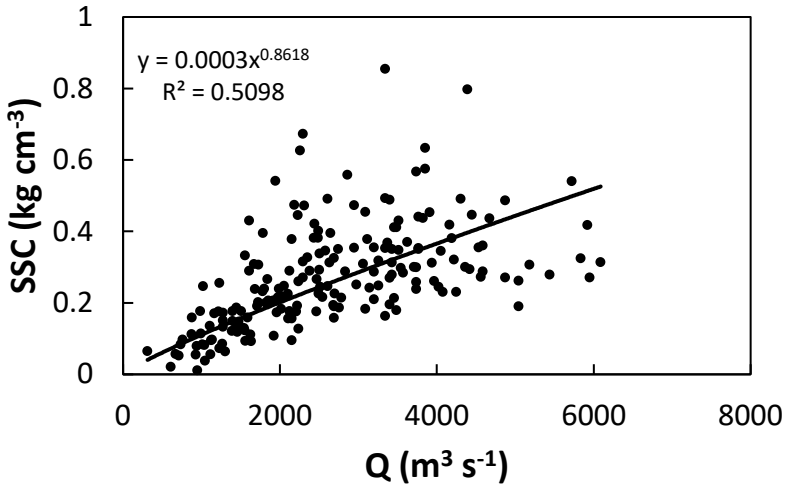

Figure A1 – Measured water discharge and suspended sediment concentration observed at the USGS Calumet gauge (Gauge 07381590) in the WLO. We use the empirically derived relationship to set the concentration of silt entering the domain at the upstream boundary of our model runs.

Acknowledgements

This work was supported by National Science Foundation grant 1812019, National Science Foundation grant, 1426997, and National Science Foundation grant 1135427. All data will be made available upon publication through the IU ScholarWorks repository http://scholarworks.iu.edu. We could like to thank Deon Knights for assistance with field work and the Coastal Systems Ecology Lab at Louisiana State University for access to data collected by observation platforms located in the Wax Lake Delta and maintenance of said platforms.

Citations

Allison, M. A., Demas, C. R., Ebersole, B. A., Kleiss, B. A., Little, C. D., Meselhe, E. A., ... & Vosburg, B. M. (2012). A water and sediment budget for the lower Mississippi–Atchafalaya River in flood years 2008–2010: implications for sediment discharge to the oceans and coastal restoration in Louisiana. *Journal of Hydrology*, *432*, 84-97.

Allison, M. A., Yuill, B. T., Meselhe, E. A., Marsh, J. K., Kolker, A. S., & Ameen, A. D. (2017). Observational and numerical particle tracking to examine sediment dynamics in a Mississippi River delta diversion. *Estuarine, Coastal and Shelf Science*, *194*, 97-108.

Baptist, M. J. (2005). Modelling floodplain biogeomorphology.

Bevington, A. E., Twilley, R. R., Sasser, C. E., & Holm Jr, G. O. (2017). Contribution of river floods, hurricanes, and cold fronts to elevation change in a deltaic floodplain, northern Gulf of Mexico, USA. *Estuarine, Coastal and Shelf Science*, *191*, 188-200.

Blum, M. D., & Roberts, H. H. (2009). Drowning of the Mississippi Delta due to insufficient sediment supply and global sea-level rise. *Nature Geoscience*, *2*(7), 488.

674 Carle, M. V., Sasser, C. E., & Roberts, H. H. (2015). Accretion and vegetation community
675 change in the Wax Lake Delta following the historic 2011 Mississippi River
676 flood. *Journal of Coastal Research*, *31*(3), 569-587.

677 Childers, D. L., & Day, J. W. (1990). Marsh-water column interactions in two Louisiana
678 estuaries. I. Sediment dynamics. *Estuaries*, *13*(4), 393-403.

679 Christiansen, T., Wiberg, P. L., & Milligan, T. G. (2000). Flow and sediment transport on a tidal
680 salt marsh surface. *Estuarine, Coastal and Shelf Science*, *50*(3), 315-331.

681 Couvillion, B. R., Barras, J. A., Steyer, G. D., Sleavin, W., Fischer, M., Beck, H., ... & Heckman,
682 D. (2011). Land area change in coastal Louisiana from 1932 to 2010.

683 CPRA. (2017). Louisiana's Comprehensive Master Plan for a Sustainable Coast. Coastal
684 Protection and Restoration Authority of Louisiana, Baton Rouge, LA. pp. 171.

685 Day, J. W., Britsch, L. D., Hawes, S. R., Shaffer, G. P., Reed, D. J., & Cahoon, D. (2000).
686 Pattern and process of land loss in the Mississippi Delta: a spatial and temporal analysis
687 of wetland habitat change. *Estuaries*, *23*(4), 425-438.

688 Day, J. W., Boesch, D. F., Clairain, E. J., Kemp, G. P., Laska, S. B., Mitsch, W. J., ... &
689 Simenstad, C. A. (2007). Restoration of the Mississippi Delta: lessons from hurricanes
690 Katrina and Rita. *science*, *315*(5819), 1679-1684.

691 Day, J. W., Kemp, G. P., Reed, D. J., Cahoon, D. R., Boumans, R. M., Suhayda, J. M., &
692 Gambrell, R. (2011). Vegetation death and rapid loss of surface elevation in two
693 contrasting Mississippi delta salt marshes: The role of sedimentation, autocompaction
694 and sea-level rise. *Ecological Engineering*, *37*(2), 229-240.

695

696 Day, J., Cable, J., Lane, R., & Kemp, G. (2016a). Sediment deposition at the Caernarvon
697 crevasse during the great Mississippi flood of 1927: implications for coastal
698 restoration. *Water*, *8*(2), 38.

699 Day, J. W., Agboola, J., Chen, Z., D'Elia, C., Forbes, D. L., Giosan, L., ... & Syvitski, J. (2016b).
700 Approaches to defining deltaic sustainability in the 21st century. *Estuarine, coastal and*
701 *shelf science*, *183*, 275-291.

702 Denes, T. A., & Caffrey, J. M. (1988). Changes in seasonal water transport in a Louisiana
703 estuary, Fourleague Bay, Louisiana. *Estuaries*, *11*(3), 184-191.

704 Esposito, C. R., Georgiou, I. Y., & Kolker, A. S. (2013). Hydrodynamic and geomorphic
705 controls on mouth bar evolution. *Geophysical Research Letters*, *40*(8), 1540-1545.

706 Esposito, C. R., Shen, Z., Törnqvist, T. E., Marshak, J., & White, C. (2017). Efficient retention
707 of mud drives land building on the Mississippi Delta plain. *Earth Surface*
708 *Dynamics*, *5*(3), 387-397.

709 Fabre, J. B. (2012). Sediment flux & fate for a large-scale diversion: the 2011 Mississippi River
710 Flood, the Bonnet Carré Spillway, and the implications for coastal restoration in south
711 Louisiana.

712 Fagherazzi, S., Kirwan, M. L., Mudd, S. M., Guntenspergen, G. R., Temmerman, S., D'Alpaos,
713 A., ... & Clough, J. (2012). Numerical models of salt marsh evolution: Ecological,
714 geomorphic, and climatic factors. *Reviews of Geophysics*, *50*(1).

715 Ferguson, R. I., & Church, M. (2004). A simple universal equation for grain settling
716 velocity. *Journal of sedimentary Research*, *74*(6), 933-937.

717 Gagliano, S. M., Meyer-Arendt, K. J., & Wicker, K. M. (1981). Land loss in the Mississippi
718 River deltaic plain.

719 Gedan, K. B., Kirwan, M. L., Wolanski, E., Barbier, E. B., & Silliman, B. R. (2011). The present
720 and future role of coastal wetland vegetation in protecting shorelines: answering recent
721 challenges to the paradigm. *Climatic Change*, *106*(1), 7-29.

722 Geleynse, N., Hiatt, M., Sangireddy, H., & Passalacqua, P. (2015). Identifying environmental
723 controls on the shoreline of a natural river delta. *Journal of Geophysical Research: Earth*
724 *Surface*, *120*(5), 877-893.

725 Grace, J. B. (1989). Effects of water depth on Typha latifolia and Typha domingensis. *American*
726 *Journal of Botany*, *76*(5), 762-768.

727 Hiatt, M., Snedden, G., Day, J. W., Rohli, R. V., Nyman, J. A., Lane, R., & Sharp, L. A. (2019).
728 Drivers and impacts of water level fluctuations in the Mississippi River delta:
729 Implications for delta restoration. *Estuarine, Coastal and Shelf Science*, *224*, 117-137.

730 Hoitink, A. J. F., & Jay, D. A. (2016). Tidal river dynamics: Implications for deltas. *Reviews of*
731 *Geophysics*, *54*(1), 240-272.

732 Howes, N. C., FitzGerald, D. M., Hughes, Z. J., Georgiou, I. Y., Kulp, M. A., Miner, M. D., ... &
733 Barras, J. A. (2010). Hurricane-induced failure of low salinity wetlands. *Proceedings of*
734 *the National Academy of Sciences*, *107*(32), 14014-14019.

735 Kadlec, R. H., & Wallace, S. (2008). *Treatment wetlands*. CRC press.

736 Keogh, M. E., Kolker, A. S., Snedden, G. A., & Renfro, A. A. (2019). Hydrodynamic controls on
737 sediment retention in an emerging diversion-fed delta. *Geomorphology*, *332*, 100-111.

738 Kim, W., Mohrig, D., Twilley, R., Paola, C., & Parker, G. (2009). Is it feasible to build new land
739 in the Mississippi River Delta?. *Eos, Transactions American Geophysical Union*, *90*(42),
740 373-374.

741 Kirwan, M. L., & Murray, A. B. (2007). A coupled geomorphic and ecological model of tidal
742 marsh evolution. *Proceedings of the National Academy of Sciences*, *104*(15), 6118-6122.

743 Kleinhans, M. G., de Vries, B., Braat, L., & van Oorschot, M. (2018). Living landscapes: Muddy
744 and vegetated floodplain effects on fluvial pattern in an incised river. *Earth surface*
745 *processes and landforms*, *43*(14), 2948-2963.

746 Kolker, A. S., Miner, M. D., & Weathers, H. D. (2012). Depositional dynamics in a river
747 diversion receiving basin: The case of the West Bay Mississippi River
748 Diversion. *Estuarine, Coastal and Shelf Science*, *106*, 1-12.

Lane, E. M., Restrepo, J. M., & McWilliams, J. C. (2007). Wave–current interaction: A comparison of radiation-stress and vortex-force representations. *Journal of physical oceanography*, *37*(5), 1122-1141.

Larsen, L. G. (2019). Multiscale flow-vegetation-sediment feedbacks in low-gradient landscapes. *Geomorphology*.

Leonard, L. A., & Luther, M. E. (1995). Flow hydrodynamics in tidal marsh canopies. *Limnology and oceanography*, *40*(8), 1474-1484.

Ma, H., Larsen, L. G., & Wagner, R. W. (2018). Ecogeomorphic Feedbacks that Grow Deltas. *Journal of Geophysical Research: Earth Surface*, *123*(12), 3228-3250.

Madden, C. J., Day Jr, J. W., & Randall, J. M. (1988). Freshwater and marine coupling in estuaries of the Mississippi River deltaic plain 1. *Limnology and Oceanography*, *33*(4part2), 982-1004.

Mariotti, G. (2016). Revisiting salt marsh resilience to sea level rise: Are ponds responsible for permanent land loss?. *Journal of Geophysical Research: Earth Surface*, *121*(7), 1391-1407.

Meade, R. H., & Moody, J. A. (2010). Causes for the decline of suspended-sediment discharge in the Mississippi River system, 1940–2007. *Hydrological Processes: An International Journal*, *24*(1), 35-49.

Miller, R. L., & Fujii, R. (2010). Plant community, primary productivity, and environmental conditions following wetland re-establishment in the Sacramento-San Joaquin Delta, California. *Wetlands Ecology and Management*, *18*(1), 1-16.

Morris, J. T., Sundareshwar, P. V., Nietch, C. T., Kjerfve, B., & Cahoon, D. R. (2002). Responses of coastal wetlands to rising sea level. *Ecology*, *83*(10), 2869-2877.

Nardin, W., & Edmonds, D. A. (2014). Optimum vegetation height and density for inorganic sedimentation in deltaic marshes. *Nature Geoscience*, *7*(10), 722.

Nardin, W., Edmonds, D. A., & Fagherazzi, S. (2016). Influence of vegetation on spatial patterns of sediment deposition in deltaic islands during flood. *Advances in Water Resources*, *93*, 236-248.

Neumeier, U., & Ciavola, P. (2004). Flow resistance and associated sedimentary processes in a Spartina maritima salt-marsh. *Journal of Coastal Research*, 435-447.

NOAA (2011). USGS Atchafalaya 2 LiDAR. NOAA's Ocean Service, Office for Coastal Management (OCM), Charleston, SC.

Olliver, E. A., & Edmonds, D. A. (2017). Defining the ecogeomorphic succession of land building for freshwater, intertidal wetlands in Wax Lake Delta, Louisiana. *Estuarine, Coastal and Shelf Science*, *196*, 45-57.

Ortiz, A. C., Roy, S., & Edmonds, D. A. (2017). Land loss by pond expansion on the Mississippi River Delta Plain. *Geophysical Research Letters*, *44*(8), 3635-3642.

786 Paola, C., Twilley, R. R., Edmonds, D. A., Kim, W., Mohrig, D., Parker, G., ... & Voller, V. R.
787 (2011). Natural processes in delta restoration: Application to the Mississippi
788 Delta. *Annual review of marine science*, *3*, 67-91.

789 Partheniades, E. (1965). Erosion and deposition of cohesive soils. *Journal of the Hydraulics*
790 *Division*, *91*(1), 105-139.

791 Perez, B. C., Day Jr, J. W., Rouse, L. J., Shaw, R. F., & Wang, M. (2000). Influence of
792 Atchafalaya River discharge and winter frontal passage on suspended sediment
793 concentration and flux in Fourleague Bay, Louisiana. *Estuarine, Coastal and Shelf*
794 *Science*, *50*(2), 271-290.

795

796 Peyronnin, N., Caffey, R., Cowan, J., Justic, D., Kolker, A., Laska, S., ... & Visser, J. (2017).
797 Optimizing sediment diversion operations: working group recommendations for
798 integrating complex ecological and social landscape interactions. *Water*, *9*(6), 368.

799 Roberts, H. H., Coleman, J. M., Bentley, S. J., & Walker, N. (2003). An embryonic major delta
800 lobe: A new generation of delta studies in the Atchafalaya-Wax Lake Delta system.

801 Rosen, T., & Xu, Y. J. (2013). Recent decadal growth of the Atchafalaya River Delta complex:
802 Effects of variable riverine sediment input and vegetation succession. *Geomorphology,*
803 *194*, 108-120.

804 Rosenheim, B. E., Roe, K. M., Roberts, B. J., Kolker, A. S., Allison, M. A., & Johannesson, K.
805 H. (2013). River discharge influences on particulate organic carbon age structure in the
806 Mississippi/Atchafalaya River System. *Global Biogeochemical Cycles*, *27*(1), 154-166.

807 Sendrowski, A., & Passalacqua, P. (2017). Process connectivity in a naturally prograding river
808 delta. *Water Resources Research*, *53*(3), 1841-1863.

809 Shaw, J. B., Mohrig, D., & Whitman, S. K. (2013). The morphology and evolution of channels
810 on the Wax Lake Delta, Louisiana, USA. *Journal of Geophysical Research: Earth*
811 *Surface*, *118*(3), 1562-1584.

812 Shaw, J. B., Ayoub, F., Jones, C. E., Lamb, M. P., Holt, B., Wagner, R. W., ... & Mohrig, D.
813 (2016). Airborne radar imaging of subaqueous channel evolution in Wax Lake Delta,
814 Louisiana, USA. *Geophysical Research Letters*, *43*(10), 5035-5042.

815 Shen, Z., Törnqvist, T. E., Mauz, B., Chamberlain, E. L., Nijhuis, A. G., & Sandoval, L. (2015).
816 Episodic overbank deposition as a dominant mechanism of floodplain and delta-plain
817 aggradation. *Geology*, *43*(10), 875-878.

818 Smith, J. E., Bentley, S. J., Snedden, G. A., & White, C. (2015). What role do hurricanes play in
819 sediment delivery to subsiding river deltas?. *Scientific reports*, *5*, 17582.

820 Snedden, G. A., Cable, J. E., Swarzenski, C., & Swenson, E. (2007). Sediment discharge into a
821 subsiding Louisiana deltaic estuary through a Mississippi River diversion. *Estuarine,*
822 *Coastal and Shelf Science*, *71*(1-2), 181-193.

Stanley, D. J., & Warne, A. G. (1993). Nile Delta: recent geological evolution and human impact. *Science*, *260*(5108), 628-634.

Stern, M. K., Day, J. W., & Teague, K. G. (1991). Nutrient transport in a riverine-influenced, tidal freshwater bayou in Louisiana. *Estuaries*, *14*(4), 382-394.

Stumpf, R. P. (1983). The process of sedimentation on the surface of a salt marsh. *Estuarine, Coastal and Shelf Science*, *17*(5), 495-508.

Syvitski, J. P., Vörösmarty, C. J., Kettner, A. J., & Green, P. (2005). Impact of humans on the flux of terrestrial sediment to the global coastal ocean. *science*, *308*(5720), 376-380.

Syvitski, J. P., & Saito, Y. (2007). Morphodynamics of deltas under the influence of humans. *Global and Planetary Change*, *57*(3-4), 261-282.

Temmerman, S., Bouma, T. J., Govers, G., Wang, Z. B., De Vries, M. B., & Herman, P. M. J. (2005). Impact of vegetation on flow routing and sedimentation patterns: Three-dimensional modeling for a tidal marsh. *Journal of Geophysical Research: Earth Surface*, *110*(F4).

Temmerman, S., Bouma, T. J., Van de Koppel, J., Van der Wal, D., De Vries, M. B., & Herman, P. M. J. (2007). Vegetation causes channel erosion in a tidal landscape. *Geology*, *35*(7), 631-634.

Turner, R. E., Baustian, J. J., Swenson, E. M., & Spicer, J. S. (2006). Wetland sedimentation from hurricanes Katrina and Rita. *Science*, *314*(5798), 449-452.

Van Heerden, I. L., & Roberts, H. H. (1988). Facies development of Atchafalaya Delta, Louisiana: a modern bayhead delta. *AAPG Bulletin*, *72*(4), 439-453.

Wang, J., Xu, K., Restreppo, G. A., Bentley, S. J., Meng, X., & Zhang, X. (2018). The coupling of bay hydrodynamics to sediment transport and its implication in micro-tidal wetland sustainability. *Marine Geology*, *405*, 68-76.

Weerman, E. J., Van Belzen, J., Rietkerk, M., Temmerman, S., Kéfi, S., Herman, P. M. J., & de Koppel, J. V. (2012). Changes in diatom patch-size distribution and degradation in a spatially self-organized intertidal mudflat ecosystem. *Ecology*, *93*(3), 608-618.

Wright, L. D., & Coleman, J. M. (1972). River delta morphology: wave climate and the role of the subaqueous proffile. *Science*, *176*(4032), 282-284.

Wright, L. D., & Coleman, J. M. (1973). Variations in morphology of major river deltas as functions of ocean wave and river discharge regimes. *AAPG Bulletin*, *57*(2), 370-398.

Wright, L. D. (1977). Sediment transport and deposition at river mouths: a synthesis. *Geological Society of America Bulletin*, *88*(6), 857-868.

Xing, F., Syvitski, J. P., Kettner, A. J., Meselhe, E. A., Atkinson, J. H., & Khadka, A. K. (2017). Morphological responses of the Wax Lake Delta, Louisiana, to Hurricanes Rita. *Elementa Science of the Anthropocene*.

Xu, K., Bentley, S. J., Day, J. W., & Freeman, A. M. (2019). A review of sediment diversion in the Mississippi River Deltaic Plain. *Estuarine, Coastal and Shelf Science*.

Yamasaki, T. N., de Lima, P. H., Silva, D. F., Cristiane, G. D. A., Janzen, J. G., & Nepf, H. M. (2019). From patch to channel scale: The evolution of emergent vegetation in a channel. *Advances in Water Resources*, *129*, 131-145.

Yang, S. L., Zhang, J., Zhu, J., Smith, J. P., Dai, S. B., Gao, A., & Li, P. (2005). Impact of dams on Yangtze River sediment supply to the sea and delta intertidal wetland response. *Journal of Geophysical Research: Earth Surface*, *110*(F3).

Yang, S. L., Li, H., Ysebaert, T., Bouma, T. J., Zhang, W. X., Wang, Y. Y., ... & Ding, P. X. (2008). Spatial and temporal variations in sediment grain size in tidal wetlands, Yangtze Delta: On the role of physical and biotic controls. *Estuarine, Coastal and Shelf Science*, *77*(4), 657-671.